Optimal Design of Resonant Converter for Electrostatic Precipitators

Thiago Soeiro*, Jürgen Biela*, Jonas Mühlethaler*, Jörgen Linnér**, Per Ranstad**, and Johann W. Kolar*
* Power Electronic Systems Laboratory, ETH Zürich, Physikstrasse 3, CH-8092 Zürich, Switzerland
** Alstom Power Sweden AB, Kvarnvägen P. O. Box 1233, SE-351 12 Växjö, Sweden

***Abstract*--This work presents a design optimization procedure for Series Parallel Resonant Converters (LCC) employed in Electrostatic Precipitator (ESP) power supplies. The system parameters, such as resonant tank elements, are selected in order to reduce semiconductor losses when a typical ESP energization operation range is considered. Here, the sum of the power losses of the switches are predicted for a set of parameters by mathematical models of the LCC resonant converter, and also by loss characteristics of suitable commercially available IGBTs obtained from experimental analysis and datasheet values. The analysis comprises two different control strategies: the conventional Variable Frequency (VF) control and the Dual Control (DC). Finally, the circuit operation and design are verified with a 60kW charging capability LCC resonant converter test set-up. Both control strategies are analyzed by comparing semiconductor's losses for five commercial modules.**

***Index Terms*—Electrostatic precipitators, genetic algorithms, LCC resonant converter.**

I. Introduction

Due to increasing concerns about environmental pollution, the reduction of particle emissions by Electrostatic Precipitators (ESPs) is a highly important issue for coal fired power plants. An ESP consists of parallel electrodes that use electrostatic charges to separate particles in the entering gas (see Fig. 1) [1].

Due to the high voltage level requirements on the ESP, $30kV_{dc}$ to $100kV_{dc}$, a transformer with a high turn ratio and with sufficient insulation between the windings is commonly used [2]. Therefore, the transformer's parasitics elements, such as leakage inductance L_σ and parallel capacitance C_P, are not negligible.

Topologies for ESP applications advantageously could utilize the parasitic elements of the transformer in order to improve the circuit operation. Thus, modern ESP power supplies are often based on a resonant converter; whose characteristics allow utilization of the transformer's parasitics into the circuit operation and have soft-switching for a wide operating range [2-6].

Fig. 1 shows the circuit of a typical ESP power supply employing a Series Parallel Resonant Converter (LCC) with capacitive output filter. The capacitor C_0 represents the electrical capacitance of the precipitator, which depends mainly on the geometric layout, dimensions and, to some extent, on the dielectric properties of the processed gas [7]. The non-linear resistance R_0 depends on the particle transport in the electrical field, and its value is inversely proportional to the particle loading [7].

For the design of the LCC converter, global optimization methods, such as the Genetic Algorithm (GA), are particularly useful due to the nature of the solution space, where the converter's parameters are strongly interdependent and many constraints must be fulfilled [8]. Therefore, a GA is developed and presented in this paper to optimally design the ESP's LCC resonant converter, resulting in high power density and lower circuit component stresses. Here, the optimized function is based on the mathematical model of the LCC converter (cf. [9]), and measured loss characteristics of commercially available IGBTs. The proposed idea reduces the design effort significantly by identifying the characteristic of the candidate parameters of the converter with the accurate model built. Thus, simulation verification steps which are normally required in traditional methods [5] [9] [10] are not necessary. The study comprises two control strategies: the conventional Variable Frequency (VF) control and the Dual Control (DC) [11].

In Section II, typical ESP operation modes and the characteristics of the two proposed control strategies for the LCC converter, VF and DC controls, are shown. Section III presents the LCC converter analytical model and means to evaluate its performance regarding

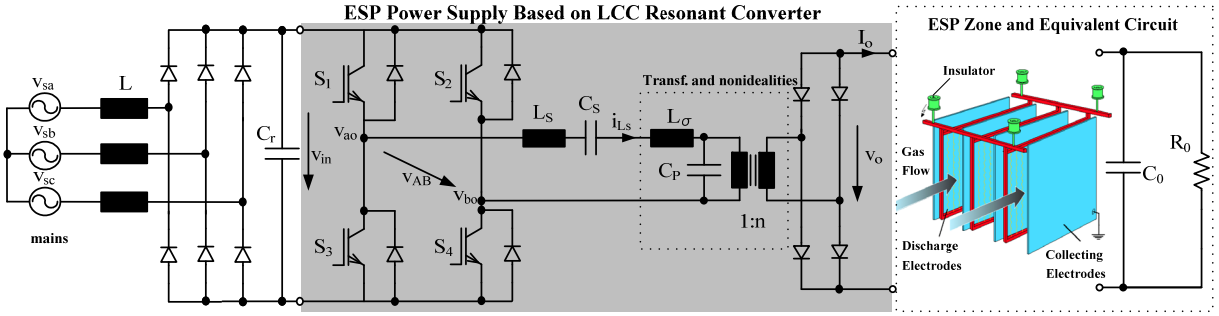

Fig. 1. Modern ESP power supplies based on LCC resonant converter

semiconductor losses for operation with VF or DC controls. In Section IV, a novel and relatively simple design procedure for LCC resonant converters based on a set of rules, which are determined by the application requirements, is presented. The proposed ESP power supply design comprises both operation in pulsed mode and continuous energization with/without flashovers. The structure of the built GA optimizer is shown and its characteristics detailed. In Section V the circuit operation and design are verified with a 60kW LCC converter test set-up, where both studied control strategies are compared by analyzing power losses of the IGBT modules.

II. ESP Power Supply Operation Modes

The ESP power supply depicted in Fig. 1 is based on a LCC resonant converter. This topology can incorporate the parasitic elements of the transformer in the circuit operation, and also can have soft-switching for a wide operation range [2-6].

The power losses in the LCC resonant converter components are strongly dependent on the ESP operation mode and the control strategy of this converter. As presented in the following, two suitable control strategies are selected and studied for the LCC converter operating with switching frequency above the resonance frequency: VF and DC control [11].

A. ESP Typical Operation Modes

ESPs are normally divided into several sections or zones for increasing the particle collection efficiency [7]. These zones have different electrical behavior and efficiency, due to: different dust loads of the zones; particle size and properties; and the possibility of charging particles in the entire zone using appropriate technology *e.g.* pulsed or continuous energization [7].

The continuous energization is usually applied where the particle concentration is very high (first zones). In order to achieve optimal precipitation efficiency, the ESP must operate at a dc voltage level very close to the flashover limit. Frequent flashovers may happen in this operating mode and a de-ionization time is needed to prevent repetitive sparks [12]. A flashover is the ESP's flowing gas dielectric breakdown, which results in a short-circuit of the power supply output.

In pulsed operation, the ESP is fed with periodic high-voltage pulses, which improves the collection efficiency of high resistivity dusts and reduces energy consumption [12]. The circuit presented in Fig. 1 is suitable for both energization techniques, but adaption of the output control reference signal is needed. In order to collect fine particles more efficiently, the output reference signal of a pulsed power supply is normally adjusted to be higher than one which would operate in continuous mode.

B. LCC Converter: Variable Frequency Control (VF)

The impedance of the resonant tank is controlled by changing the inverter's switching frequency to above the resonant frequency. While switches in one leg maintain a 50% duty cycle, the switches of the other leg are 180° phase shifted (cf. Fig. 2(a)).

The converter operation above resonance is desired, because the four transistors commutate with Zero Voltage Switching (ZVS). The switches turn on when the anti-parallel diodes are conducting and turn off with current. Therefore, losses are generated in the turn-off process and lossless snubber capacitors are commonly employed.

One drawback of the VF control is that normally it requires a high switching frequency to reach low output current operation. Moreover, it suffers from high switching losses at high current and low output voltage operation, due to a triangular current-waveform, with turning off at the peak [11]. The large frequency variation makes it more difficult to optimize the magnetic components, gate circuitry, and the EMI filters. Some benefits of the VF control are simple operation, limited number of operation modes, and an even loss distribution between the switches [11].

C. LCC Converter: Dual Control (DC)

The converter's output power is controlled by duty-cycle variation and the operation frequency is automatically adjusted to ensure the commutation of one bridge leg at zero current (ZCS) and the other bridge leg at zero voltage (ZVS) (cf. Fig. 2(b)).

One advantage of using DC control strategy is the possibility of employing two different switch technologies, due to its inherit loss characteristics. For example, one could utilize transistors with low

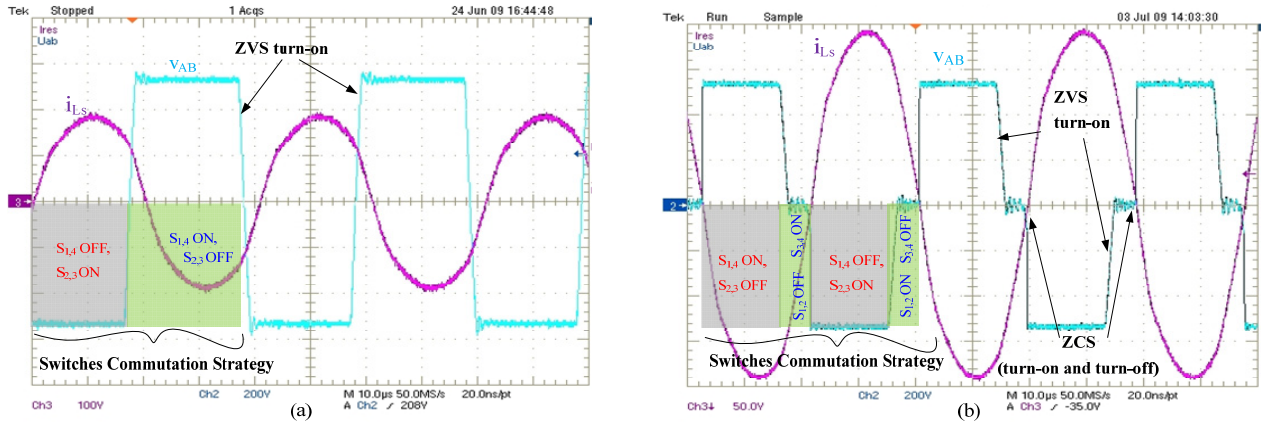

Fig. 2. 60kW LCC converter experimental results: resonant current i_{Ls} and inverter output voltage for (a) VF control, (b) DC control. Note that, i_{Ls} signal is inverted.

conduction losses on the ZCS leg, and switches with low turn off losses features on the ZVS leg. Ideally the diodes D_2 and D_4 never conduct, however, in practical implementation the commutation cannot be triggered exactly at zero current and a dead-time between both switches is necessary. Thus, D_2 and D_4 have to be implemented but they conduct only for a very short time [5].

A drawback of this strategy is an uneven current distribution between both legs of the full-bridge inverter. This leads to higher conduction losses in the switches that are synchronized with the zero crossing of the resonant current compared with the ZVS switches of the other leg [5]. This is due to the fact that the ZCS switches are conducting current almost 50% of the switching period, while the turn-on interval of the ZVS switches is dependent on the duty cycle [5].

III. LCC Converter: Loss Prediction Model

In this section, the LCC converter analytical model and means to evaluate its performance regarding semiconductor losses for operation with VF or DC controls are presented.

A. Loss Prediction Model

Based on the first harmonic analysis [9], the equations describing the LCC converter behavior are derived for VF and DC control strategies (cf. (1)-(12)). The stress on all converter power components can be calculated by (13)-(25). Here, the expressions of electrical current through the semiconductors as a function of the operating point, given by the phase displacement ϕ between the first harmonic of the inverter output voltage, and the resonant current and/or the inverter duty cycle D are particularly interesting. Combining these expressions with the loss characteristics of commercially available IGBTs one can predict the total semiconductor losses which a converter has for a specific arrangement of components. In this way, the loss prediction model is built and used in an optimization strategy in order to optimally design the LCC converter for minimal semiconductor losses.

Eqs. (28)-(31) describe the semiconductor losses for VF control, where V_{meas} represents the link voltage used to extract the loss model. For DC control the semiconductor power losses are given by (32)-(37), where E_{optm} is the optimal switching energy for ZCS bridge leg (cf. Fig. 9).

The semiconductor power loss model is obtained according to [13]. The loss model is described with dependency on the instantaneous current I_C through the semiconductor and the turn-off current I_{C_off} as shown in (26) and (27). a_i, b_i and c_i are the 2nd order equation fitting coefficients obtained by data-sheet and/or experimental analysis. Due to their low turn-off energy and conduction loss characteristics, five commercially available power modules were selected as candidates for use in the 60kW prototype. A test set-up was built to experimentally obtain the switching loss characteristics of these power modules for ZVS and ZCS switching (cf. Fig. 3). To guarantee current measurements with fast response and high bandwidth, a current transformer was designed. The IGBT was assembled on an aluminium plate which is thermally isolated from the large cooling plate. The aluminium plate is electrically grounded. Additionally, two power resistors were assembled to heat this small plate to a defined temperature (e.g. 125° C). Fig. 4 shows the experimented circuit diagrams for the ZVS and ZCS switching.

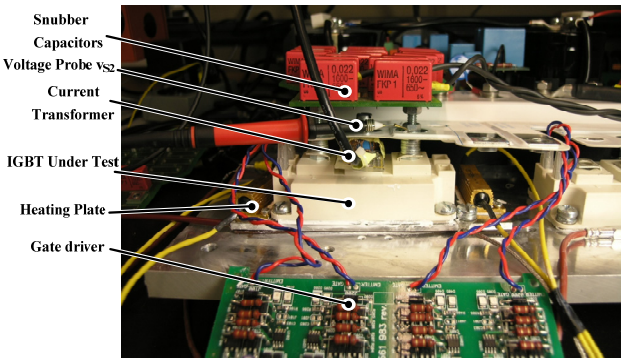

Fig. 3. Test set-up used to extract the switching loss characteristics of the IGBTs under analysis.

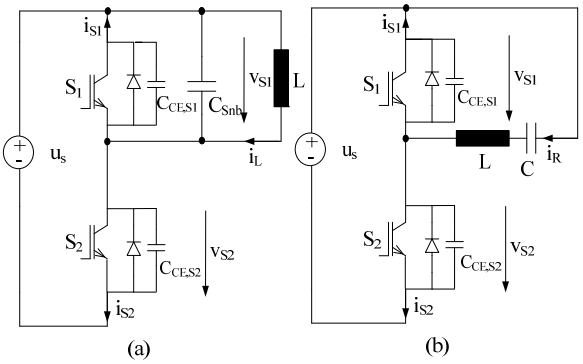

Fig. 4. Test circuits for (a) ZVS and (b) ZCS switching loss characteristics.

In the ZVS test circuit, turning on the IGBT S_2 applies a constant voltage across the inductor L, which results in a linear increase of the current i_L. Turning off S_2 forces the current i_L into the parasitic collector emitter capacitors C_{CE} of the two IGBTs S_1 and S_2, and if assembled, into the snubber capacitor C_{Snb}. After the capacitor $C_{CE,S2}$ is charged to the value of the supply voltage (and therewith $v_{S1} = 0$), the freewheeling diode of the IGBT S_1 starts conducting. Here, the switching power loss is calculated as the integral of the product of the instantaneous current $i_{S2}(t)$ and the instantaneous voltage $v_{S2}(t)$. The integration starts when the voltage v_{S2} exceeds a threshold of 20 V and it is ended at the beginning of the turn off oscillations, when the power oscillates, i.e. it has positive and negative values. In Fig. 5, measured typical current and voltage waveforms are plotted for the turning off process. All measurements were repeated at two different junction temperatures ($T_j = 25^oC$ and $T_j = 125^oC$) and with different snubber capacitor values. Fig. 6 shows the results for the IGBT #1 with different values of snubber capacitors and $T_j = 125^oC$. In Fig. 7, the results for all analyzed semiconductors are summarized in a bar chart for $T_j = 125^oC$ and $C_{Snb}=396nF$.

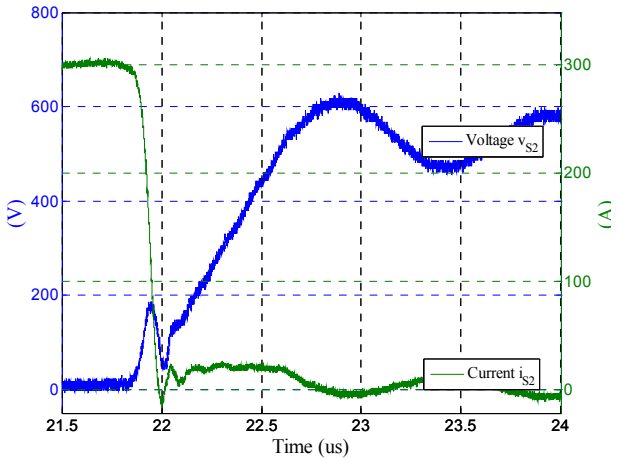

Fig. 5. Turn off measured waveforms with snubber capacitor C_{Snb}=396nF.

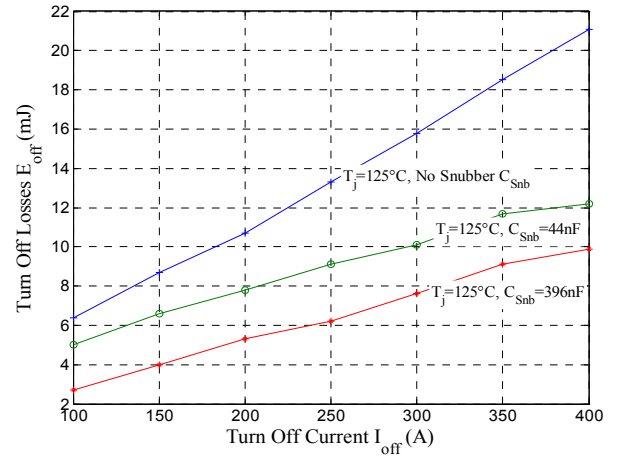

Fig. 6. IGBT #1 ZVS turn off measurement results for different C_{Snb}.

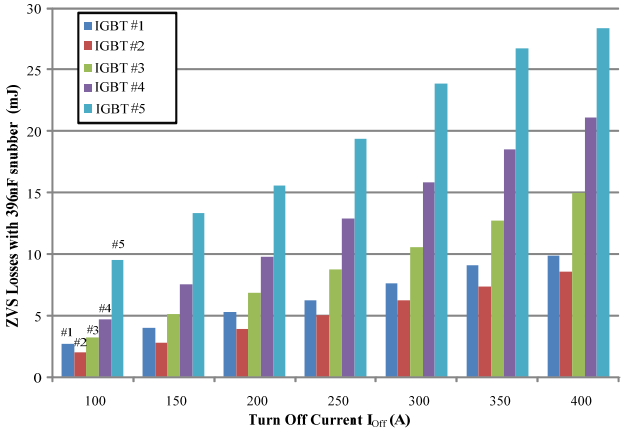

Fig. 7. ZVS turn off measurement results, T_J= 125°C and C_{Snb}=396nF.

For the ZCS test circuit, turning S_2 on applies a constant voltage across the resonant tank, so that the current i_R follows a sinusoidal oscillation. As soon as the current i_{S2} decreases to a certain value I_{off}, S_2 is turned off. Ideally, the system waits until the current reaches zero and then triggers the switching event. In reality, switching at exactly zero current is not desirable. After S_2 is turned off, the current i_R flows via the internal parasitic capacitances of the IGBT S_1 and S_2. As soon as the capacitances are charged/discharged, the freewheeling diode of S_1 starts conducting. Then, a lossless ZVS turn on of S_1 is possible. Turning S_2 off earlier means turning off at high current, resulting in high turn off losses. Turning S_2 off later reduces losses, but the corresponding low current i_R may not be sufficient to fully discharge/charge the capacitances of S_1/S_2 within the dead time t_d. Hence, turn on losses occur because of the stored energy in the internal parasitic capacitance $C_{CE,S1}$, that is not fully discharged. Therefore, there is an ideal turn off current I_{off}, which results in minimal losses. In Fig. 8, measured current and voltage waveforms are plotted, where the current i_R at turn off was not sufficient to fully charging/discharging the IGBTs' internal capacitances.

The ZCS commutation loss characteristic obtained for the IGBT #1 is shown in Fig. 9, where special attention has to be paid to the optimal current commutation point for ZCS, with dependency on the junction temperature T_j and the bridge-leg dead time t_d. In Fig. 10 the results for all analyzed IGBTs are summarized in a bar chart for optimal t_d.

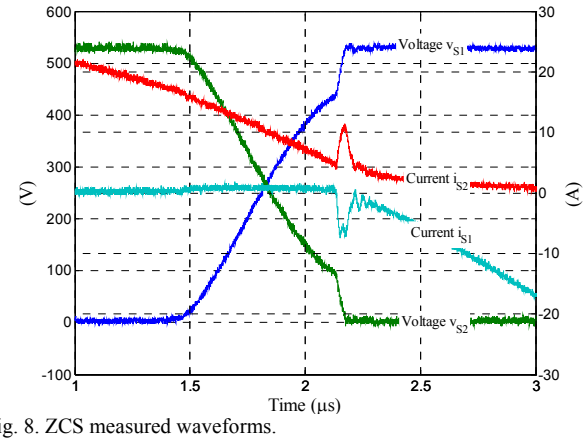

Fig. 8. ZCS measured waveforms.

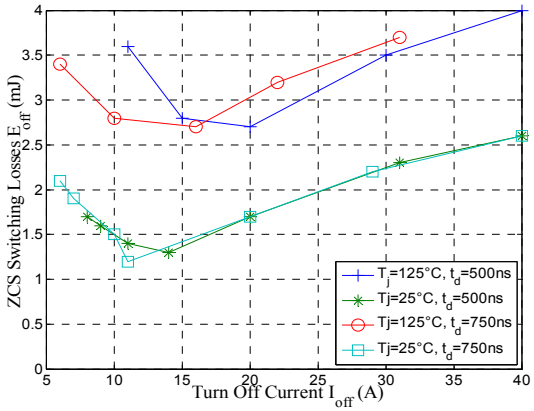

Fig. 9 –ZCS switching loss characteristics.

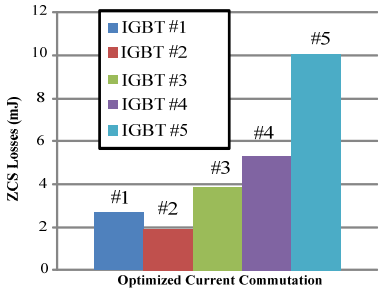

Fig. 10 – ZCS losses, T_J = 125°C and t_d= optimal.

IV. LCC CONVERTER: DESIGN PROCEDURE

In this section, a relatively simple design procedure for LCC resonant converters based on a set of rules, which are determined by the application requirements, is presented. A GA is developed to optimally design the ESP's LCC resonant converter, resulting in high power density and lower circuit component stresses.

The proposed ESP power supply design comprises both the ESP operation modes and the control strategy used for the LCC converter (VF or DC controls).

A. LCC Resonant Converter Design Procedure

Often modern ESP power supplies are based on the LCC resonant converter (cf. Fig. 1), which is designed to provide a steady output over a wide range of output power (P_0) and input voltage (V_{in}) [11]. This ensures operation above resonance to enable soft-switching. The output current (I_0) is the variable which directly determines the ESP collection efficiency, and for this reason it is normally feedback controlled. In this work, a bandwidth-limited design methodology is used, where the converter's performance with a set of parameters is evaluated, regarding semiconductor losses, in a specified operation range.

A LCC converter design procedure based on genetic algorithms is proposed. The sum of semiconductor power losses for five operating points are predicted for a set of circuit parameters (C_P, α, f_s and n) by analyzing the mathematical model of the LCC resonant converter (cf. [9]) and the semiconductor characteristics obtained from experimental analysis. The optimal set of parameters is determined by tracking the minimal power losses of the semiconductors, when the input voltage of the converter and power capability are defined.

From the first harmonic analysis of the system operating behavior [9], one obtains for a defined control strategy (VF or DC control), output voltage V_0 and output current I_0, the set of equations (1) to (12). These equations are condensed into a nonlinear equation $V_0=f(V_0, I_0, f_{sN})$, which is used to numerically determine a unique $f_{sN}=f_s/f_o$, by combining the set of parameters (C_P, α, f_s, n), with the specified operation condition for maximum loading P_{0max} and minimum input voltage V_{in_min}. The necessary resonant circuit elements, L_s and C_s, to fulfill this operation are then calculated.

With the LCC converter components designed and with a specific operation point given by V_{in}, V_0 and I_0, a unique f_{sN}, ϕ, D and f_s can be found. Hence, the converter performance for an operation range can be predicted by evaluating the stress on all power components (cf. (13)-(25)) and the losses on the module semiconductors (cf. VF control (28)-(31) and DC control (32)-(37)).

A function which adds up the semiconductors' power losses obtained for the set of parameters (C_P, α, f_s, n) in five operation points is used to assign a value to this designed LCC converter. This function is minimized by an optimization strategy based in genetic algorithms. Weighting factors can be utilized to give to the analyzed operation points different degrees of importance.

A flowchart describing the design optimization strategy and the 60kW prototype specifications are shown in Fig. 11.

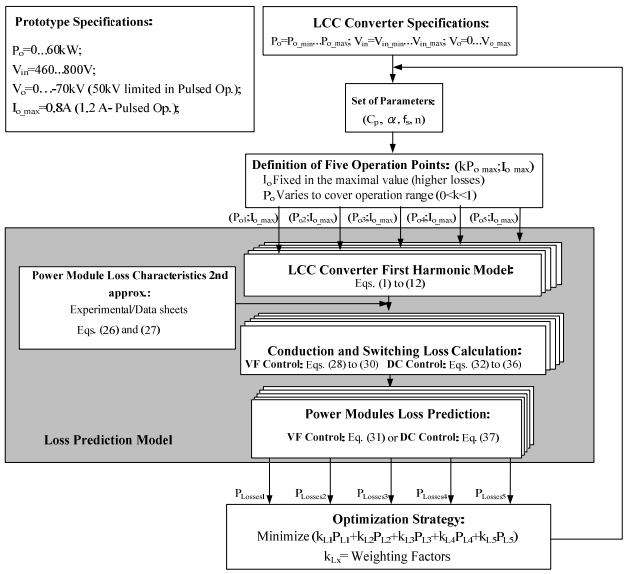

Fig.11. LCC converter design strategy flowchart. Equations (1) to (37) are presented in the appendix.

The restriction or requirements for this application are translated as optimization constraints, which are described as follows:

- Switching frequency f_s is limited to $f_{smax}>f_s>f_{smin}$. The bottom limit f_{smin}, which can be reached mainly in pulsed mode, is selected as compromise between audible noise and volume of passive elements. The upper limit f_{smax} is determined by the power semiconductor switching loss, gate drive and signal electronics delay times on the operating behavior. The maximal switching frequency can be reached at high input voltage and/or low power operation (i.e. during flashovers).
- The maximum voltage stress on the series capacitor C_s has to take into consideration the range of capacitor technology available for high frequency and high-current applications.
- The capacitance of the parallel resonant capacitor C_P, has to take into consideration the minimum achievable winding capacitance of the high transformer employed in the case at hand. The upper limit is determined by the converter operating range, which is strongly dependent on $\alpha=C_P/C_S$ [5]. For lower values of α, the frequency range will be wider than for higher values. Note that, as the parallel capacitance (C_P) is a geometrically dependent parameter, a desired value can be obtained by optimally designing the transformer dimensions [14-17].
- The series inductance L_S can be set to be smaller than the maximal achievable leakage inductance (L_σ) of the transformer. If this condition is not satisfied, a penalty can be added to the GA fitness function.
- The minimum transformer turn ratio n is determined according to the minimal input, V_{in_min}, and maximal output voltages at full power. If a small n value is used

a lower current would flow in the main circuit, thereby lowering the losses. However, this could mean the system operates at switching frequencies close to resonance f_o. To preserve the desired soft-switching, the normalized frequency must fulfil $f_{sN}=f_s/f_o>1$ [3]-[5]. Note that, for the power supply depicted in Fig. 1, V_{in_min} has to consider not only the minimal allowed mains' voltage operation, but also the drop of link's voltage which is expected in pulsed operation.

- The squared error between the design specification point and candidate point is used to add a penalty to the optimized function, e.g. if V_o cannot be reached.

B. Optimization Strategy Based on Genetic Algorithms

A flowchart shown the complete structure of the developed genetic-algorithm optimizer is presented in Fig. 12.

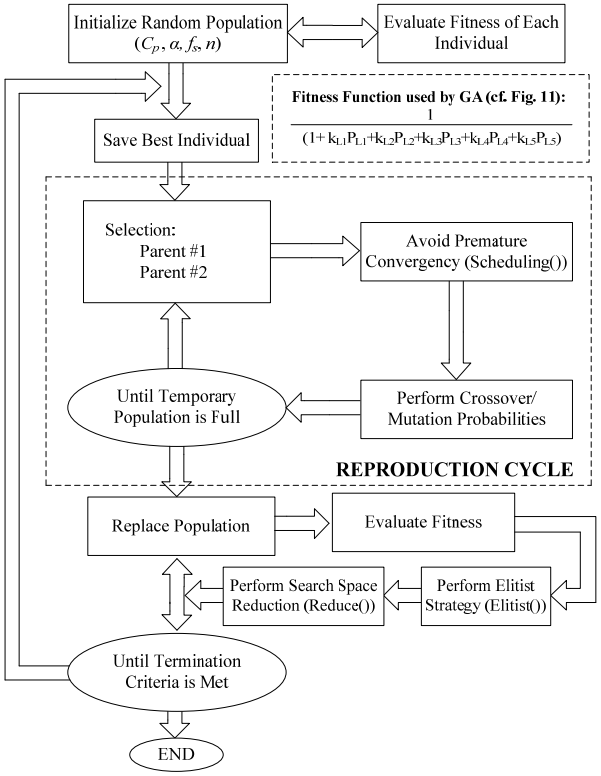

Fig. 12. Complete structure of the built GA. Ref. to [8], [18-21].

During the GA optimization, a set of trial solutions, or individuals, is chosen, and for each one a fitness value is assigned by evaluating the fitness function. For the LCC converter design each individual is represented by a set of parameters that are regarded like the genes of a chromosome (C_p, α, f_s, n).

In each cycle of genetic operation a subsequent generation (offspring) is created from the chromosomes in the current population (parent). The genes of the parents are mixed and recombined for the production of offspring in the next generation [18]. An operation rate (p_{cross}) is used as the probability of crossover. In order to facilitate the GA evolution cycle, a mutation function is used to perturb the mated population [18]. It is expected that from this process of evolution (manipulation of genes), the "better" chromosome will create a larger number of offspring, and thus has a higher chance of surviving in the subsequent generation, emulating the survival-of-the-fittest mechanism in nature [18]. Fitness values are evaluated for, and assigned to, each of the new individuals. The termination criterion is then evaluated.

The functions Scheduling(), Elitist() and Reduce() are used to improve the convergence of the GA. For more details in genetic algorithms theory, [8] and [18-21] are recommended.

V. Experimental Verification

In order to determine the most suitable IGBT power module and control strategy for the LCC resonant converter specified project, first the built GA optimizer was used to obtain a set of optimized parameters (C_p, α, f_s, n), and to predict losses for both VF and DC controls (see Appendix). To validate the calculations, the losses for the power IGBT modules are evaluated in a 60kW test set-up converter. The experimental system and the circuit diagram are shown in Fig. 13 and 14. Therein, the transformer with high turns ratio was replaced by a 1:1 transformer. This system consists of a LCC resonant and a regenerative boost converter, where the latter acts as an electronic load and also feeds the output power back to the dc link of the main converter. In this way, the power supply is used only to compensate the system losses. The IGBT losses are measured calorimetrically, by measuring the rise in temperature of the cooling water, which is circulated at a constant flow rate. The resonant components were selected to be the same for all control strategies and power semiconductors, as a compromise between all the GA optimal results. Thus, for a specific operation point and control technique, each analyzed module commutates at similar switching frequency, giving similar stress to the other circuit elements. Fig. 2 shows the resonant current i_{Ls} and the inverter's output voltage obtained experimentally for VF and DC controls.

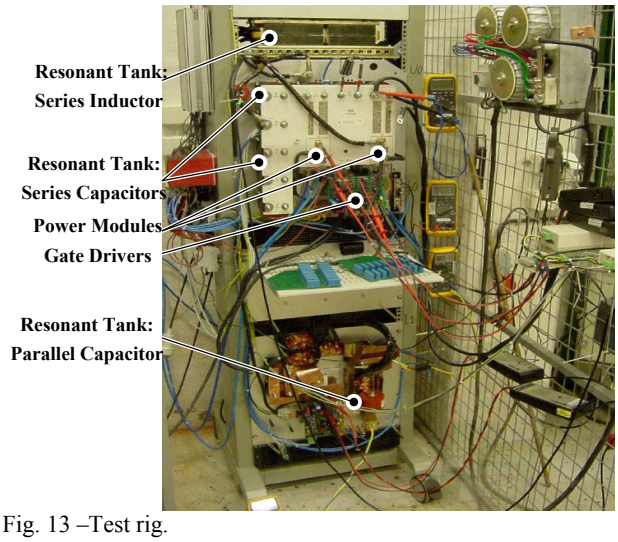

Fig. 13 –Test rig.

For the sake of brevity, the loss model verification (experimental results/model prediction) is shown in Fig. 15 only for the IGBT #3 module; however the same accuracy (±5%) is obtained for the other IGBTs. Fig. 15

also presents the comparative results for three of the power modules tested and the control strategies studied. The analyses are made in continuous operation mode at constant current of 120A and for different output voltages, 0 to 485V. A graph comparing the results for the semiconductor that obtained the highest losses against that with the best loss results in the considered voltage range is depicted in Fig. 15. As one can observe, the power loss reduction can range from 160W to 660W, for maximum and minimum power loading respectively.

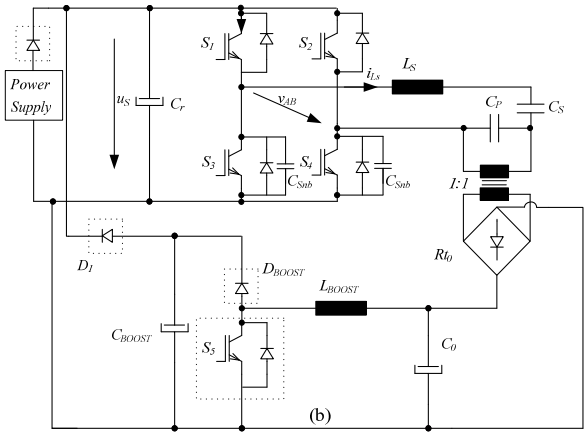

Fig. 14 – Test rig circuit diagram.

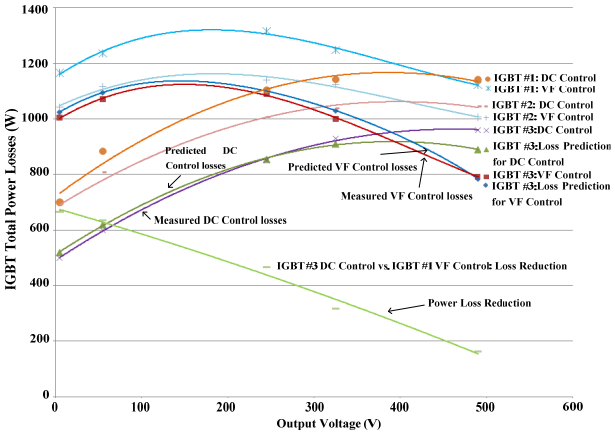

Fig. 15. Power loss model verification and loss results.

VI. Conclusions

As one can observe in Fig. 15, the power module loss model is very accurate (±5%), this justifies its use in optimally designing the LCC resonant converter. One can also observe that for each commercial power module there is a region where VF control would be preferable (full power operation) and another region where DC control has better results (operation < $70\%P_{o\_max}$). However, due to the high flashover rate (output short-circuit rate), which can be around 10 to 50 times per second, and also the variation of dust concentration in the ESP zones, the power supplies operate for a considerable time in the region $<70\%P_{o\_max}$, even when they are set to deliver full power. In this way, the most suitable control technique for this application is the DC control, but one has to accept the uneven distribution of losses among the bridge-legs, which may occur.

Appendix

From the first harmonic analysis of the system operating behavior, one obtains for a defined control strategy (VF or DC control), output voltage V_0 and output current I_0, the set of equations (1) to (12) [9]. These equations can be condensed into a nonlinear equation $V_0=f(V_0,\ I_0,\ f_{sN})$, which can be used to numerically determine a unique f_{sN}, by combining a set of parameters (C_p, α, f_s, n), with the specified operation condition for maximum loading P_{0max} and minimum input voltage V_{in_min}. The necessary resonant circuit elements, L_s and C_s, to fulfill this operation can then be calculated.

With the LCC converter components designed and with a specific operation point given by V_{in}, V_0 and I_0, a unique f_{sN}, ϕ, D and f_s can be found. Hence, the converter performance for an operation range can be predicted by evaluating the stress on all power components (cf. (13)-(25)) and the losses on the module semiconductors (cf. VF control (28)-(31) and DC control (32)-(37)).

Characteristic impedance	$Z_s = \sqrt[2]{L_s/C_s}$	(1)
Series resonant frequency	$f_0 = \frac{1}{2\pi\sqrt[2]{L_s C_s}}$	(2)
Normalized switching frequency	$f_{s,N} = \frac{f_s}{f_0}$	(3)
Ration between the parallel and series capacitances	$\alpha = \frac{C_p}{C_s}$	(4)
Rectifier conduction angle	$\theta = 2\tan^{-1}\sqrt{\frac{\pi n^2 Z_s I_0}{2f_{s,N}\alpha V_0}}$	(5)
Ratio of V_o and peak of the 1st harm. of the primary voltage	$k_v = 1 + 0.27\sin\left(\frac{\theta}{2}\right)$	(6)
Displacement of the fundamental voltage and current on the primary side	$\beta = -0.4363\sin(\theta)$	(7)
Dimensionless parameter	$\omega C_p R_e = \frac{\pi {k_v}^2}{4\left(\tan\left(\frac{\theta}{2}\right)\right)^2}$	(8)
$k_{21} = \frac{1}{\sqrt{\left[1-\alpha(f_{s,N}^2-1)\left(1+\frac{\tan(\lvert\beta\rvert)}{\omega C_p R_e}\right)\right]^2 + \left[\frac{\alpha}{\omega C_p R_e}(f_{s,N}^2-1)\right]^2}}$		(9)
$\phi = \tan^{-1}\left(\frac{\alpha}{\omega C_p R_e}\left(f_{s,N}^2\left(1+[\omega C_p R_e+\tan(\lvert\beta\rvert)]^2-1\right)\right) - [\omega C_p R_e+\tan(\lvert\beta\rvert)]\left[1+\alpha\left(1+\frac{\tan(\lvert\beta\rvert)}{\omega C_p R_e}\right)\right]\right)$		(10)

	VF Control	DC Control	
duty cycle	D=1	$D=1-\frac{2}{\pi}\phi$	(11)
V_0 function	$\frac{V_0}{nV_{in}} = \frac{4}{\pi}\frac{k_{21}}{k_v}\sin\left(D\frac{\pi}{2}\right)$		(12)
1st harm. peak of the I_{Ls}	$I_{Ls\,pk} = \frac{2f_{s,N}\alpha}{n(1+\cos(\theta))}\frac{V_0}{Z_s}$		(13)
1st harm. peak of the V_{Ls}	$V_{Ls\,pk} = I_{Ls\,pk} 2\pi f_s L_s$		(14)
1st harm. peak of V_{Cs}	$U_{Cs\,pk} = \frac{I_{Ls\,pk}}{2\pi f_s C_s}$		(15)
Average (Avg) input current I_{in_avg}	$\frac{2I_{Ls\,pk}}{\pi}\cos(\phi)$	$\frac{I_{Ls\,pk}}{\pi}(1-\cos(D\pi))$	(16)
ZVS leg turn-off current	$I_{Ls\,pk}\sin(\pi-\phi)$	$I_{Ls\,pk}\sin(D\pi)$	(17)

	VF Control	DC Control	
RMS current on the ZVS leg transistors I_{C_RMS}	$\frac{I_{Ls\,pk}}{2} * \sqrt{\frac{\pi-\phi}{\pi} - \frac{\sin(2(\pi-\phi))}{2\pi}}$	$\frac{I_{Ls\,pk}}{2}\sqrt{D - \frac{\sin(2D\pi)}{2\pi}}$	(18)
RMS current on the ZVS leg diodes I_{D_RMS}	$\frac{I_{Ls\,pk}}{2} * \sqrt{\frac{\phi}{\pi} + \frac{\sin(2(\pi-\phi))}{2\pi}}$	$\frac{I_{Ls\,pk}}{2} * \sqrt{1 - D + \frac{\sin(2D\pi)}{2\pi}}$	(19)
Avg current on the ZVS leg transistors	$\frac{I_{Ls\,pk}}{\pi}(\cos(\frac{\phi}{2}))^2$	$\frac{I_{Ls\,pk}}{2\pi}(1 - \cos(D\pi))$	(20)
Avg current on the ZVS leg diodes	$\frac{I_{Ls\,pk}}{\pi}(\sin(\frac{\phi}{2}))^2$	$\frac{I_{Ls\,pk}}{2\pi}(1 + \cos(D\pi))$	(21)
ZCS leg RMS current	-	$I_{C\_RMS} = \frac{I_{Ls\,pk}}{2}$	(22)
ZCS leg Avg current	-	$I_{C\_avg} = \frac{I_{Ls\,pk}}{\pi}$	(23)
Transform primary RMS current	$I_{T1\,rms} = I_0 \frac{n\sqrt[2]{2}}{k_v \cos\beta}$		(24)
output diodes currents	$I_{D\,rms} = \frac{I_0}{k_v \cos\beta}$ and $I_{D\,avg} = \frac{I_0}{2}$		(25)
Conduct. loss	$P_{cond} = a_C . {I_C}^2 + b_C . I_C + c_C$ [W]		(26)
Switching loss	$K_{IGBT} = a_S . {I_{C\_off}}^2 + b_S . I_{C\_off} + c_S$ $[\frac{\mu Ws}{A}]$ $P_{Swt} = E . f_S = K_{IGBT} . I_{C\_off} . f_S . 10^{-6}$[W]		(27)
$P_{T\_Cond} = \frac{1}{2\pi}[a_{TC}{I_{Lspk}}^2\left(\frac{\pi-\phi}{2} - \frac{\sin(2(\pi-\phi))}{4}\right) + 2b_{TC}I_{Lspk}(\cos(\frac{\phi}{2}))^2 + 2\pi c_{TC}]$			(28)
$P_{D\_Cond} = \frac{1}{2\pi}[a_{DC}{I_{Lspk}}^2\left(\frac{\phi}{2} + \frac{\sin(2(\pi-\phi))}{4}\right) + 2b_{DC}I_{Lspk}(\sin(\frac{\phi}{2}))^2 + 2\pi c_{DC}]$			(29)
$P_{T\_Swtch} = \frac{V_{in} I_{C\_off} f_S 10^{-6}}{V_{meas}}[a_S {I_{C\_off}}^2 + b_S I_{C\_off} + c_S]$			(30)
$P_{Total} = 4[P_{T\_Cond} + P_{D\_Cond} + P_{T\_Swtch}]$			(31)
$P_{T\_ZVS\_Cond} = \frac{1}{2\pi}[a_{TC}{I_{Lspk}}^2\left(\frac{D\pi}{2} - \frac{\sin(2\pi D)}{4}\right) + b_{TC}I_{Lspk}(1 - \cos(D\pi)) + 2\pi c_{TC}]$			(32)
$P_{D\_ZVS\_Cond} = \frac{1}{2\pi}[a_{DC}{I_{Lspk}}^2\left(\frac{(1-D)\pi}{2} + \frac{\sin(2\pi D)}{4}\right) + b_{DC}I_{Lspk}(1 + \cos(D\pi)) + 2\pi c_{DC}]$			(33)
$P_{T\_ZVS\_Swtch} = \frac{V_{in} I_{C\_off} f_S 10^{-6}}{V_{meas}}[a_S {I_{C\_off}}^2 + b_S I_{C\_off} + c_S]$			(34)
$P_{T\_ZCS\_Cond} = \frac{1}{2\pi}[\frac{\pi a_{TC}{I_{Lspk}}^2}{2} + 2b_{TC}I_{Lspk} + 2\pi c_{TC}]$			(35)
$P_{T\_ZCS\_Swtch} = E_{optm} f_S$			(36)
$P_{Total} = 2[P_{Tzvs_{Cond}} + P_{Dzvs_{Cond}} + P_{Tzvs_{Swtch}} + P_{T\_ZCS\_Cond} + P_{T\_ZCS\_Swtch}]$			(37)

REFERENCES

[1] P. Ranstad, C. Mauritzson, M. Kirsten, and R. Ridgeway, "On experiences of the application of high-frequency power converters for ESP energization," *International Conference on Electrostatic Precipitation ICESP 2004*.

[2] G. Demetriades, P. Ranstad, C. Sadarangari, "Three elements resonant converter: The LCC topology by using MATLAB," *Power Electronics Specialists Conference,* Vol.2, pp.1077-1083, 2000.

[3] P. Ranstad, and G. Dementriades, "On Conversion Losses in SLR and LCC-topologies," IEE MED POWER 2002, Athens, Greece.

[4] T. Melaa, A. K. Ådnanes, K. Öye, T. F. Nestli, R. Nilsen, P.Ranstad, "Evaluation of resonant converters for increased soft switching range," *European Conference on Power Electronics and Applications,* EPE 97.

[5] F. S. Cavalcante, and J. W. Kolar, "Design of a 5kW High Output Voltage Series-Parallel Resonant Converter," *Proceedings of the 34th IEEE Power Electronics Specialists Conference*, Vol. 4, pp. 1807-1814, 2003.

[6] P. Ranstad, and K. Porle, "High frequency power conversion: A new technique for ESP energization," *EPRI/DOE 1995*, August 1995.

[7] N. Grass, "Fuzzy Logic-Optimising IGBT Inverter for Electrostatic Precipitators," *IEEE- Industry Applications Conference*, Vol. 4, pp. 2457-2462, October 1999

[8] D. E. Goldberg. *Genetic Algorithms in Search, Optimization and Machine Learning*. Addilson-Weslley, New York, 1989.

[9] G. Ivensky, A. Kats, S. Ben-Yaakov, "A Novel RC Model of Capacitive-Loaded Parallel and Series-Parallel Resonant DC-DC Converters," *Proceedings of the 28th IEEE Power Electronics Specialists Conference*, pp. 958-964, 1997.

[10] A. K. S. Bhat, "A Resonant Converter suitable for 650 V DC bus Operation," *IEEE Transaction on Power Electronics* Vol. 6, no. 4, pp. 739-748, 1991.

[11] P. Ranstad, H. P. Nee, J. Linner, "A novel control strategy applied to the series loaded resonant converter," *Conf. on Power Elect. and Applic.(EPE)* pp. 1–10, Dresden, 2005.

[12] N. Grass; W. Hartmann, "Application of Different Types of High-Voltage Supplies on Industrial ESP," *IEEE Transaction On Industrial Application*, Vol. 40 no 6, December 2004.

[13] U. Drofenik and J. W. Kolar, "A General Scheme for Calculating Switching- and Conduction- Losses of Power Semiconductors in Numerical Circuit Simulations of Power Electronic Systems", IPEC, Niigata, Japan, 2005.

[14] J. P. Vandelac, P. Ziogas, "A novel approach for minimising highfrequency transformer copper losses," *IEEE Power electronics specialists conference record* 1987, pp. 355-367.

[15] V.A Niemela, G.R. Skutt, A.M. Urling, Y.N. Chang, T.G. Wilson, H.A. Owen, Jr., R..C. Wong, "Calculating the short-circuit impedances of a multi-winding transformer from its geometry," *IEEE, Power Elect. Spec. Conf. PESC* 1989.

[16] R. Prieto, R. Asensi, J.A. Cobos, O. Garcia, J. Uceda, "Model of the capacitive effects in the magnetic components," *IEEE, Power Elect. Spec. Conf. PESC* 1995

[17] Y. Kim, H. Hatakeyama and M, Nakaoka, "Comparative Evaluations of Phase-Shifted PWM Resonant Inverter- fed DC-DC Converter with High-Voltage High-Frequency Transformer Link", ," *IEEE, Power Elect. Spec. Conf. PESC*,Vol. 1, pp. 120-127, 1995.

[18] J. Michael, and Y. Rahmat, "Genetic Algorithms in Engineering Electromagnetics," *IEEE Antennas and Propagation Magazine*, Vol. 39, pp. 7-21, August 1997.

[19] J. A. Vasconcelos, J. A. Ramirez, R. H. C. Takahashi, R. R. Saldanha, "Improvements in Genetic Algorithms," *IEEE Transaction On Magnetics*, Vol. 37 No. 5, September 2001.

[20] K. F. Man, K. S. Tang, S. Kwong, "Genetic Algorithms: Concepts and Applications." *IEEE Transaction On Industrial Electronics*, Vol. 43 No 5, October 1996.

[21] J. L. Ribeiro, P. C. Treleaven, C. Alippi "Genetic-Algorithm programming Environments" *Computer*, Vol. 27 No 6, pp. 28-43, June 1994.